Journal of Electroanalytical Chemistry 823 (2018) 128–136

Contents lists available at ScienceDirect

Journal of Electroanalytical Chemistry

journal homepage: www.elsevier.com/locate/jelechem

# Mesoporous NiPh/carbon fibers nanocomposite for enhanced electrocatalytic oxidation of ethanol

Reham H. Tammam[a], A.H. Touny[b,c], Mamduoh E. Abdesalam[c], M.M. Saleh[a,c,*]

[a] Department of Chemistry, Faculty of Science, Cairo University, Cairo, Egypt
[b] Department of Chemistry, Faculty of Science, Helwan University, Helwan, Egypt
[c] Chemistry Department, College of Science, King Faisal University, Al-Hassa, Saudi Arabia

ARTICLE INFO

*Keywords:*
Nickel
Fibers
Phosphate
Ethanol
Mesoporous

ABSTRACT

Mesoporous nickel phosphate/carbon fibers nanocomposite (Nano-CF/NiPh) shows Type IV isotherm with H4 hysteresis loop as evident form $N_2$ adsorption/desorption measurements. NiPh is fabricated by cost-effective reflux method and the crystalline mesoporous structure is proved by different surface and structure instrumentations including [Brunauer-Emmett-Teller] surface area measurements, transmission electron micrograph with selected-area electron diffraction, FE-SEM and XRD. Impregnation of CF (20% by weight) onto the NiPh powder has found great impacts on the surface, electrochemical and catalytic characteristics of the Nano-CF/NiPh. This is attributed to the enhanced specific surface area of Nano-CF/NiPh (84.3 $m^2 g^{-1}$) compared to NiPh (19.0 $m^2 g^{-1}$) and to the increase in the electrochemically active surface area. Electrochemical oxidation of ethanol on the Nano-CF/NiPh has shown better performance than electrocatalysts cited in literatures. Important kinetic and transport parameters have been calculated and compared with literatures. The process takes advantages of the mesoporous structure of the NiPh, high electronic conductivity of the CF and the stability of the phosphate matrix.

## 1. Introduction

Alkaline fuel cells (AFCs) have gained considerable attentions during the last decades due to enhanced kinetics of the fuel oxidation and oxygen reduction reaction (ORR) compared to those in acidic solutions [1–4]. Pt-based catalysts suffer from poisoning and high cost limitations [5, 6]. Thus, partial or full replacement of the Pt and Pt-based electrocatalysts can be a target for many researchers [7–9]. The above considerations enabled the researchers to use non-noble metals and metals oxides such as (Ag, Ni, Co and Mn) as electrocatalysts in such AFCs [10, 11]. One more advantage of using alcohol as the fuel in what is so called direct alcohol fuel cells (DAFCs) is the easiness of handling such liquids (e.g., $CH_3OH$ (MeOH) or $C_2H_5OH$ (EtOH)) and easiness of storage. The use of EtOH as a fuel has more advantages over methanol since it gives higher energy density, higher solubility and also it is more available and is considered to be non-toxic liquid. In this context, many researchers have paid more attention to direct ethanol fuel cells (DEFCs) since they have potential technological aspects and can present alternative power source for domestic and portable devices [12, 13]. However, one of the most important challenges (among other challenges including engineering and marketing challenges) is the design of efficient and cost-effective electrocatalysts for such fuel cells.

Pt and Pt-based catalysts have been the best catalysts for electrochemical oxidation of EtOH in alkaline electrolytes. However, they suffer from their high cost and low tolerance to CO poisoning [14, 15]. Several non-noble oxides such as NiO, $Co_2O_3$ and MnO (as examples) have been used for electrochemical oxidation of ethanol from alkaline solutions for full or partial replacement of Pt-based electrocatalysts [16–18]. Among those metal oxide nanoparticles modified electrodes, Ni- and NiO-based electrodes have extensively used for electrochemical oxidation of methanol [19–21] and ethanol [22–25] in alkaline solutions. However, less attention has been paid for using Ni-salt (e.g., Nickel phosphate, NiPh) that bearing redox couple (i.e., Ni(II) and Ni (III) species) as electrocatalyst for simple organic molecules. Nickel phosphate modified electrodes have great important applications such as in supercapacitors [26] and electrocatalysis [27]. Some authors used NiPh modified electrodes for electrochemical oxidation of methanol [28] and formaldehyde [29]. However, the method of synthesis was not cost-effective and the obtained performance is not unique. In this context, we prepared mesoporous NiPh in our laboratory by simple reflux method and it was applied previously for electrochemical oxidation of glucose [30] and urea [31] from alkaline solutions. However

* Corresponding author at: Department of Chemistry, Faculty of Science, Cairo University, Cairo, Egypt.
*E-mail address:* mahmoudsaleh90@yahoo.com (M.M. Saleh).

https://doi.org/10.1016/j.jelechem.2018.06.002
Received 23 March 2018; Received in revised form 27 May 2018; Accepted 1 June 2018
Available online 03 June 2018
1572-6657/ 

and since we used the material without a conducting support, the conductivity was low and the performance was acceptable but not outstanding.

Different support carbon nanomaterials have been used in literatures along with Ni-based catalysts for electrochemical oxidation of small organic molecules [32–36]. The carbon material had two functions: it increases the adsorption affinity to organic molecules and also increases the conductivity of the NiO-based matrix. It is the aim of the present work to increase the interparticles conductivity of the synthesized NiPh mesoporous material and also to increase the adsorbability to the analyte such as EtOH by fabricating a nanocomposites with carbon nanofibers. The nanocomposite will be characterized by different techniques including spectroscopic and electrochemical techniques. EtOH electrooxidation will be studied on Nano-CF/NiPh modified glassy carbon electrode in alkaline solutions. The process will be analyzed in the light of the collected experimental data. Various kinetic and transport parameters will be determined.

## 2. Experimental

### 2.1. Chemicals and synthesis procedure

Vapour-grown carbon fibers were delivered from Showa Denko Co, Ltd., USA with electrical resistivity ~0.012 Ω cm. The chemicals of high purity (analytical grade) have been purchased from Sigma-Aldrich and Fisher. They have been used without further purification (as received). All solutions were prepared using deionized water. Nickel phosphate was synthesized using a hydrothermal process based on simple reflux method. The details of the hydrothermal process can be found in our previously published work [37]. However, here in, some details will be given briefly. A precipitate of nickel phosphate was mainly prepared from nickel nitrate ($Ni(NO_3)_2.6H_2O$) and ammonium dibasic phosphate ($(NH_4)_2HPO_4$). Few drops of conc. Nitric acid were added to dissolve the precipitate and to get a uniform homogenous solution. A 50 mL of 0.3 M urea solution was added to the homogenous mixture. Refluxing of the above solution was done at 90 °C with a uniform stirring for 10 h. The obtained suspension was left to cool to room temperature, filtered and washed several times with deionized water. Finally, the precipitate was left in an oven at 100 °C to dry for overnight to be ready for different characterizations.

Preparation of the catalyst ink of NiPh, for being anchored on the surface of glassy carbon electrode (GC), was prepared by adding 12 mg of NiPh + 3 mg of CF in to a test tube containing 2.5 mL isopropanol + 50 μL of Nafion solution (5% in water). The above mixture was sonicated for 30 min in an ice bath.

### 2.2. Fabrication of the electrode

Glassy carbon, GC (*diameter* = 3 mm) is used here as the underlying substrate for the CF/NiPh composite. It was cleaned by mechanical polishing with aqueous slurries of successively finer alumina powder (down to 0.06 μm), then washed thoroughly with deionized water and then with ethanol. Next, 50 μL of a freshly prepared CF/NiPh suspension (prepared as given above) is casted onto the thus cleaned GC electrode and left overnight for drying in air. The prepared loading level is 2.5 mg $cm^{-2}$ (of the electrode surface area).

### 2.3. Measurements

High resolution transmission electron micrograph, TEM and X-ray diffraction, XRD (PANalytical, X'Pert PRO) operated with Cu target (λ = 1.54 Å) were used to identify the crystallographic structure of the nano-NiPh. XRD radiation generated at 40 kV and a current of 44 mA with a scan rate of 2°/min over a 2° range of 4–80°. The morphology of the NiPh samples was investigated using field-emission scanning electronic microscopy (SEM, Model JEOL JSM 5410, Japan). The BET specific surface area of the samples was examined using low-temperature (77.0 K) nitrogen adsorption isotherms measured over a wide range of relative pressures from 0.02 to 0.95 atm. Adsorption measurements were performed on a Micrometrics ASAP2010 volumetric adsorption apparatus. High-purity nitrogen (99.999%) was used. Prior to measurement, the samples were degassed at 40 °C for 18 h in the degas pot of the adsorption analyzer.

Electrochemical measurements were performed using Gamry potentiostat/galvanostat supported with Gamry electrochemical analysis technique. Electrochemical measurements were carried out in a conventional three-electrode cell. The counter electrode was made of a platinum coil. The reference electrode was Ag/AgCl/KCl (sat.) with a Luggin probe positioned near the electrode surface. The potential throughout the text is referred to the above reference electrode. The EIS measurements were carried out in the frequency range from 10 mHz to 100 kHz and using a signal of amplitude 5 mV peak-to-peak at the open circuit potential. The measurements were repeated to test the reproducibility of the results. Electrochemical double layer capacitance was estimated using cyclic voltammetry method (see details in the Supplementary material).

## 3. Results and discussion

### 3.1. Surface and electrochemical characterization

In this section the surface, structural and electrochemical characterizations of the Nano-CF/NiPh synthesized by the process described in the experimental section are studied. The chemical structure of the Nano-CF/NiPh material is deduced from the XRD pattern in Fig. 1. The peaks labeled in asterisk are assigned for the carbon component and the rest of peaks are for NiPh. According to the XRD pattern, the composition of the material is found to be $Ni_3(PO_4)_2.8H_2O$ with a monoclinic crystallographic form with the given characteristic peaks of the NiPh appear at 2$\theta$ values that are compatible with the standard spectrum (PDF. No. 33-0591) [38]. The XRD pattern demonstrates that the sample was formed in a single phase structure. The average grain size $D_{hkl}$ is estimated to be 80.0 nm for the NiPh prepared by the present experimental conditions. The FE-SEM image is shown in Fig. 2A. It reveals one-dimensional carbon nanofibers with dimensions of 150 nm × 1.0 μm with NiPh particles of dimensions of 150 nm × 250 nm. Also, the image shows some sheet-like shape of the NiPh of larger dimensions. The micrographs (B–D) in Fig. 2 represent TEM images (B, C) and SAED pattern (D) of the Nano-CF/NiPh. The TEM image displayed in Fig. 2B demonstrates a rod-like shape of the carbon fibers of average dimensions of ~100 nm × 1.0 μm dimensions. The particles accumulated on the CF rods are assigned for the NiPh

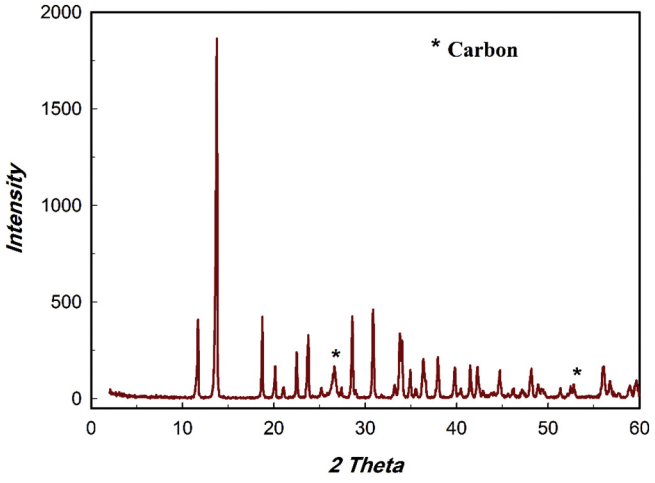


**Fig. 1.** XRD pattern of the Nano-CF/NiPh.

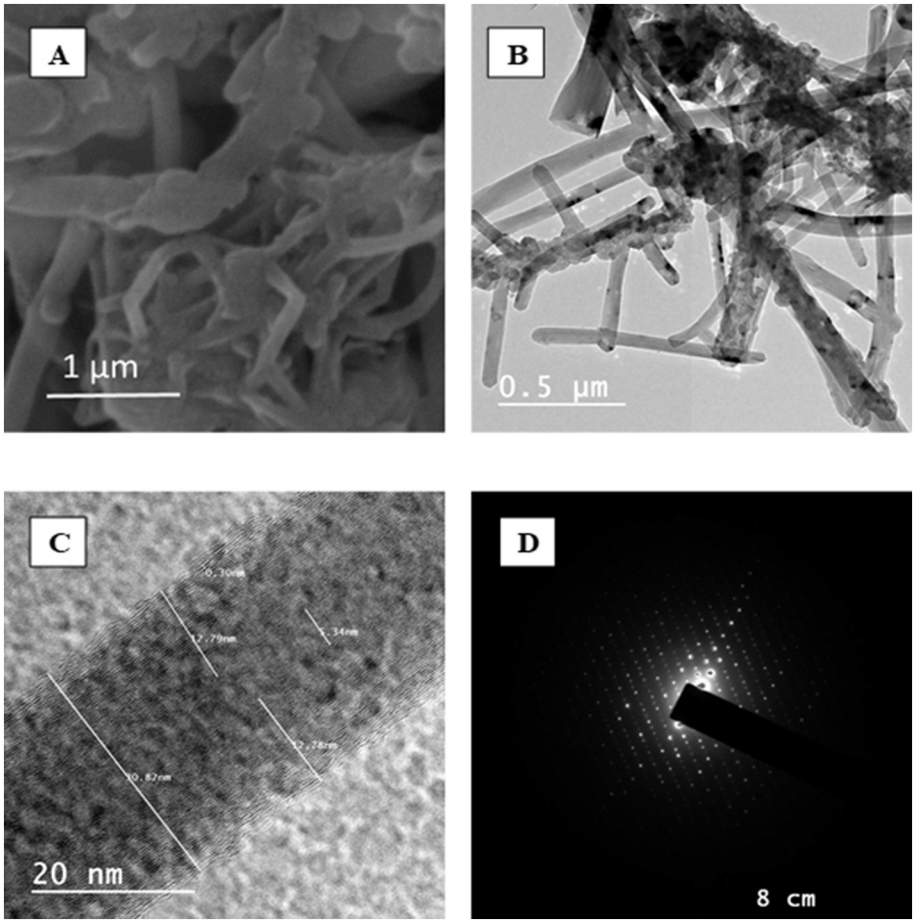


**Fig. 2.** (A) FE-SEM microimage, (B) TEM image (C) TEM image of the Nano-CF/NiPh (high magnification) and (D) Selected-area electron diffraction (SAED) pattern.

particles of average particle dimensions of 100 × 200 nm. The above image demonstrates a good impregnation of the NiPh with the CF. The roughness on the surface is attributed to the mesoporous nature of the surface. Those pores can be clarified by a magnified image as shown in Fig. 2C. The micrograph in Fig. 2C shows an average pore size of 5–10 nm. The SAED pattern is shown in Fig. 2D. The bright dots indicate a crystalline material which is consistent with the XRD pattern (see Fig. 1).

The three materials (CF, NiPh and Nano-CF/NiPh) were investigated by using nitrogen adsorption/desorption measurements. The BET (Brunauer-Emmett-Teller) calculations were applied to study the difference in specific surface area and pore diameter distributions of the above three materials. Fig. 3 shows $N_2$ adsorption/desorption isotherms of the CF (top), NiPh (middle) and Nano-CF/NiPh (bottom). In general the isotherms show type IV exhibited an H4 hysteresis loop. Type IV isotherm with H4 hysteresis loop at a relative high pressure is due to the incomplete desorption of $N_2$ from narrow slit-like pores. Type H4 hysteresis is usually represented by materials containing micro- and meso- or macroporosity such as hierarchical carbons or mesoporous zeolites. This is in accordance with IUPAC and literatures [39–41]. The insets show BJH (Barrett–Joyner–Halenda) method for the three materials. The above results indicated a mesoporous materials and lead to important parameters that are listed in Table 1. It can be seen from Table 1 that the highest surface area is for CF (128.8 $m^2 g^{-1}$) and the lowest is for NiPh (19.0 $m^2 g^{-1}$). The specific area of Nano-CF/NiPh is in between those two values (i.e., 84.3 $m^2 g^{-1}$). The above values demonstrate the impact of the CF impregnation onto the NiPh and hence the obtained high specific surface area for the Nano-CF/NiPh does enhance the electrochemical and catalytic properties of the nanocomposite (see Table 1).

Enrichment of the NiPh matrix with Ni(II)/Ni(III) redox species can be done by potential cycling of the Nano-CF/NiPh/GC electrode in 0.5 M NaOH. By the first few cycles, the obtained cyclic voltammograms (CV) (are not shown here) show one broad anodic and one cathodic peak of low currents. Upon continuous potential cycling, the peak currents of both anodic and cathodic peaks increases up to cycle number 70. The increase of the currents can be attributed to the invasion of the $OH^-$ ions to the NiPh matrix and the continuous buildup of the active nickel redox species according the following equation [42, 43];

$$Ni_3(PO_4)_2 + 3OH^- \rightarrow Ni_3(OH)_3(PO_4)_2 + 3e \quad (1)$$

In the above equation Ni(II)Ph is converted to Ni(III)Ph. For simplicity we are going to denote them as Ni(II) and Ni(III), respectively. Electrochemical impedance spectroscopy (EIS) measurements are introduced here to demonstrate the effect of compositing the CF with the NiPh matrix. Fig. 4 shows Nyquist plots of GC/nano-NiPh (a) and Nano-CF/NiPh/GC (b) at the open circuit potential. The two plots have some similarity since they both show tilted line. However, focused inspection of the two plots implies different values of the film resistance (see inset at high frequency range). The film resistance is combination of the solution resistance and the solid film (NiPh and Nano-CF/NiPh) resistance. The solution is conductive enough and hence the value of $R_s$ is a reflection of the solid film resistance. The value of $R_s$ is 25.25 and 18.0 Ω for nano-NiPh/GC and Nano-CF/NiPh/GC, respectively. This points to the higher conductivity of the Nano-CF/NiPh/GC over the nano-NiPh/GC and hence the former may offer better charge transfer in the phosphate matrix. The increase in the interparticles resistance may affect the electrochemical performance of the Nano-CF/NiPh.

Electrochemical characterization of the Nano-CF/NiPh/GC and the

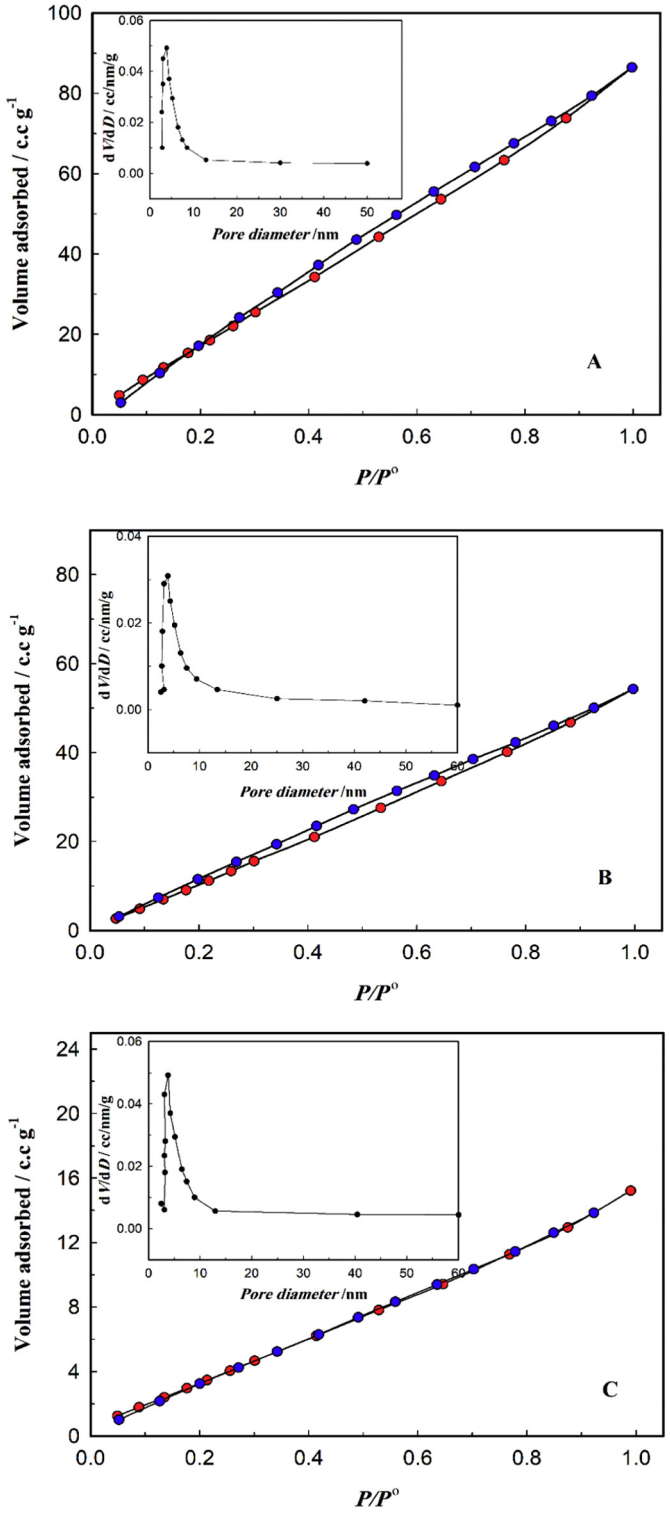


**Fig. 3.** Nitrogen adsorption/desorption isotherms and the corresponding pore size distribution plots (inset) of CF (A), Nano-CF/NiPh (B) and NiPh (C).

**Table 1**
BET and BJH parameters for CF, NiPh and Nano-CF/NiPh.

| Material | Specific surface area/ $m^2\,g^{-1}$ | Pore diameter/ nm | Pore volume/ $cm^3\,g^{-1}$ |
|---|---|---|---|
| CF | 128.791 | 3.7–8.0 | 0.114 |
| NiPh | 18.9636 | 3.7–8.0 | 0.0195 |
| Nano-CF/NiPh | 84.3053 | 3.7–8.0 | 0.0728 |

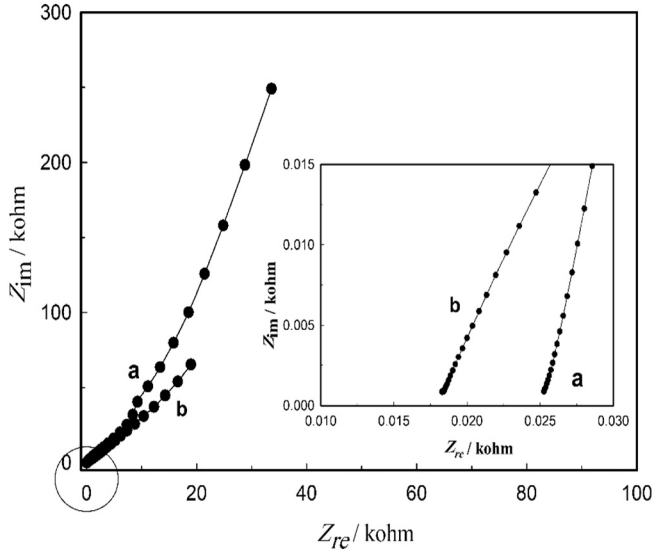


**Fig. 4.** Nyquist Plots of Nano-CF/NiPh/GC (a) and nano-NiPh/GC (b) in 0.5 M NaOH at the $E_{oc}$. The inset shows magnification of the high frequency region.

above redox couple (Ni(II)/Ni(III)) was studied by taking CV responses at different scan rates as shown in Fig. 5A. As the scan rate increases the anodic and cathodic peak currents of the Ni(II)/Ni(III) redox peak increases and also the anodic peak potential ($E_{pa}$) shifts to more positive values and the cathodic peak potential ($E_{pc}$) shifts to more negative values but with different extent than the anodic peak potential. That is to say, the peak separation, $\Delta E_p$ increase with the potential scan rate. The above results are characteristics of quasi-reversible process [44]. The above CVs at different scan rates were analyzed in order to study the nature of the Ni(II)/Ni(III) couple transformation.

At lower range of scan rates (up to 100 mV $s^{-1}$), the plots of the $I_{pa}$ and $I_{pc}$ with the potential scan rate, $\nu$ are depicted in Fig. 5B. They give straight lines in both the anodic and cathodic branches. The obtained results may be attributed to an electrochemical activity of the immobilized redox couple Ni(II)/Ni(III) at the GC electrode surface. At higher range of scan rates, (> 100–1200 mV $s^{-1}$) a plot of the $I_{pa}$ with the square root of the scan rate, $\nu^{0.5}$ gives straight line (see Fig. 5C). This signifies the fact that the dominant factor in this case is a diffusion process as the rate-limiting step in the total redox transition of the modified electrode. This diffusion-controlled process, reported for other Ni-based modified electrodes [45, 46], may be due to the charge neutralization of the film during the oxidation/reduction process [47]. It may be concluded that the redox transformation (Ni(II)/Ni(III)) inside the phosphate matrix is controlled by the diffusion of the $OH^-$ ions from solution.

### 3.2. Electrochemical oxidation of ethanol

In this section, a comparison between the performance of the Nano-CF/NiPh/GC and nano-NiPh/GC (without CF) is carried out in blank and in presence of EtOH. Fig. 6A shows cyclic voltammetry responses of the CF/GC (a, a′) and of the Nano-CF/NiPh/GC (b, b′) in blank 0.5 M NaOH (a, b) and in 0.5 M NaOH containing 0.2 M EtOH (a′, b′). In case of the CF/GC electrode, the CVs in presence and absence of EtOH do not show any characteristics features and yet it may be concluded that CF/GC is not active towards EtOH oxidation. In case of the Nano-CF/NiPh/GC electrode, the CV in blank shows the response of the redox couple Ni(II)/Ni(III) as discussed above in Fig. 5A. Similar features can be shown in Fig. 6B for nano-NiPh/GC (with the same loading of NiPh) which shows CV responses of the GC (a, a′) and of the nano-NiPh/GC (b, b′) in blank 0.5 M NaOH (a, b) and in 0.5 M NaOH containing 0.2 M EtOH (a′, b′). However, significant differences can be found between Nano-CF/

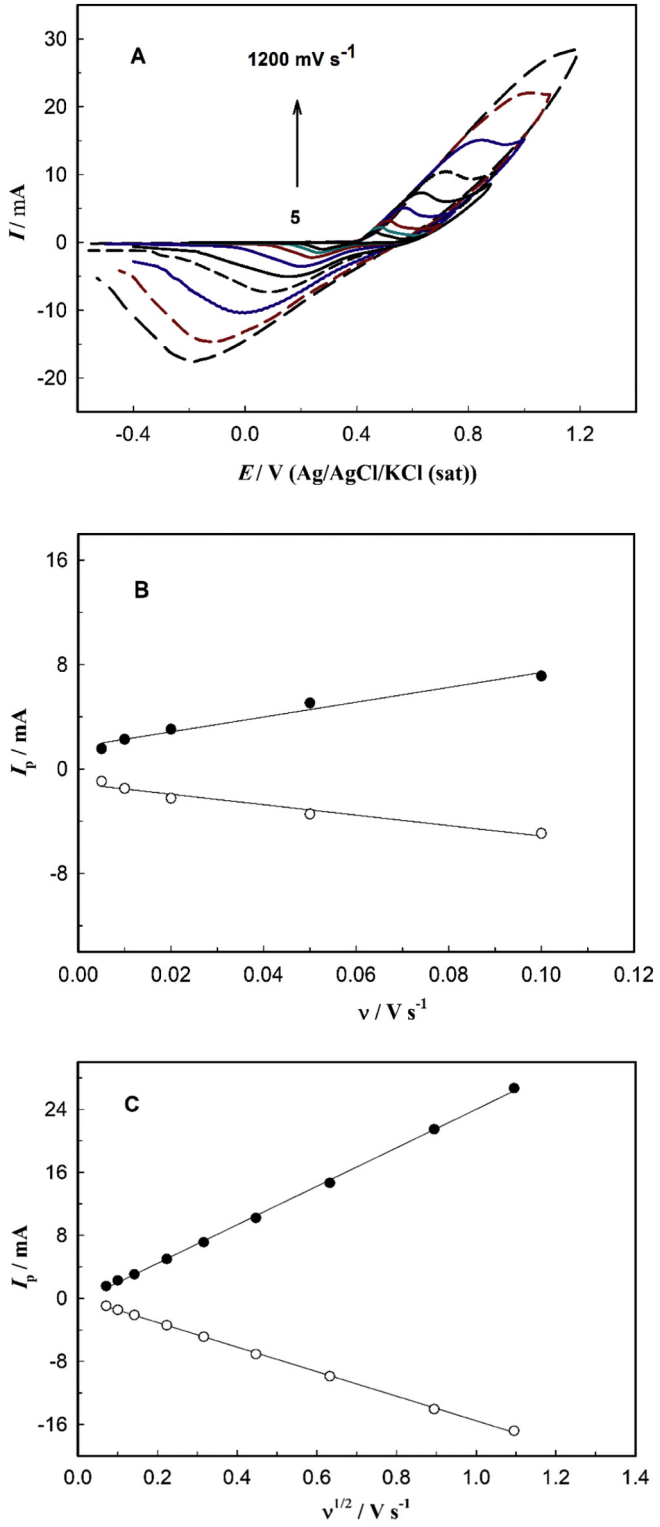


**Fig. 5.** (A) CV responses of Nano-CF/NiPh/GC in 0.5 M NaOH at different scan rates. From inner: 5, 10, 20, 50, 100, 200, 400, 800, 1200 mV $s^{-1}$. (B) Relation between $I_p$ and the scan rate, $\nu$ ($\nu < 0.1$ V $s^{-1}$), (C) between $I_p$ and the scan rate, $\nu$ ($\nu > 0.1$ V $s^{-1}$).

NiPh/GC and nano-NiPh/GC in the peak current both in blank and in presence of ethanol. The onset potential, $E_{onst}$ is little bit shift towards more negative value in case of Nano-CF/NiPh/GC. For instance, $E_{onst}$ is 0.4 V and 0.43 V for Nano-CF/NiPh/GC and nano-NiPh/GC, respectively. However, the peak current, $I_p$ in presence of EtOH is much higher in case of the Nano-CF/NiPh/GC, i.e., $I_p$ is 10-fold higher in case

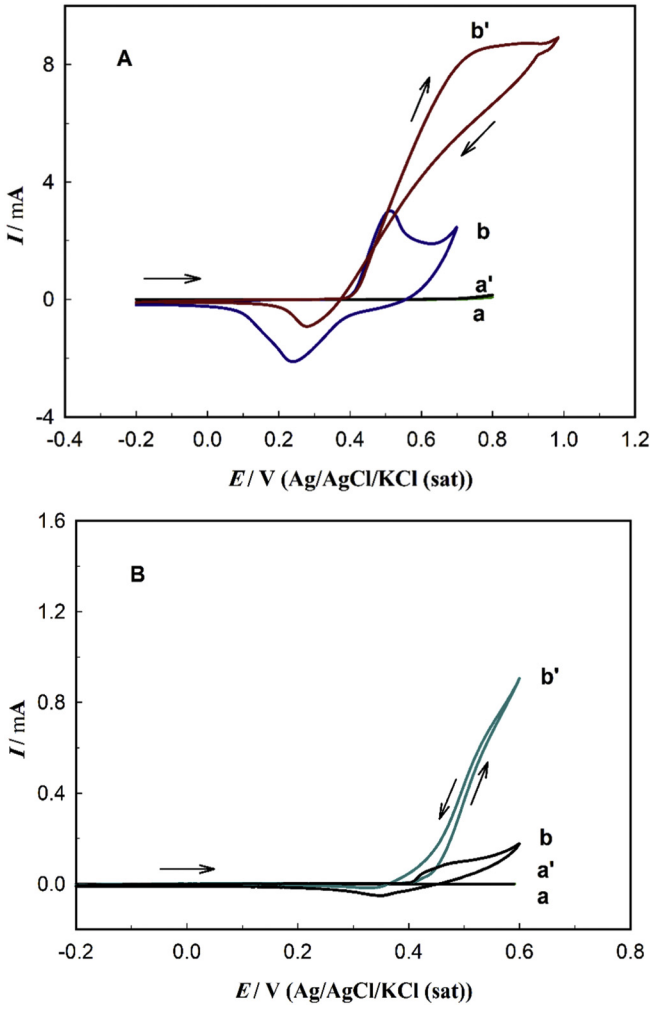


**Fig. 6.** (A) CV responses of CF/GC (a, a′) and of the Nano-CF/NiPh/GC (b, b′) in blank 0.5 M NaOH (a, b) and in 0.5 M NaOH containing 0.4 M EtOH (a′, b′). (B) CV responses of GC (a, a′) and of the nano-NiPh/GC (b, b′) in blank 0.5 M NaOH (a, b) and in 0.5 M NaOH containing 0.2 M EtOH (a′, b′).

of Nano-CF/NiPh/GC than that of nano-NiPh/GC. This can be attributed to the high surface area of the CF associated with the NiPh in the nanocomposite (see the above section). Also, the adsorption ability of the CF and synergism that may take place between NiPh and CF can be considered. One another important reason can be the tremendous increase in the concentration of the active nickel species in case of the Nano-CF/NiPh/GC. The concentration of the electroactive nickel species in the electrode matrix, $\Gamma$ can be calculated from the following equation;

$$\Gamma = \frac{Q_{tr}}{nF} \tag{5}$$

where $Q_{tr}$ is the charge passed during the Ni(II)/Ni(III) transform, $n$ is the number of electron and $F$ is Faraday's constant. The quantity of charge, $Q_{tr}$ was estimated by integrating of the area under the anodic sweep and cathodic sweep (see Fig. 5A). The value of $\Gamma$ is found to be $1.73 \times 10^{-3}$ and $5.5 \times 10^{-5}$ and mmol $cm^{-2}$ for the Nano-CF/NiPh/GC and nano-NiPh/GC, respectively. It means 20 folds increase in the concentration of electrochemically active species in the NiPh matrix. This will enhance the electrochemical reaction of ethanol on the Nano-CF/NiPh/GC electrode.

In presence of EtOH, a significant increase of the anodic peak current is observed with coincidence with the peak current of the Ni(II)/Ni (III) redox transformation. The peak current value reaches at potential

of 0.8 V. This is attributed to EtOH electrochemical oxidation on the Nano-CF/NiPh/GC electrode and hence the electrode possesses a catalytic enhancement towards EtOH oxidation at the present conditions. It can be noticed that the reduction peak current of the Ni(III) → Ni(II) transformation in the reverse sweep decreases dramatically and shifts to more positive potential. This is attributed to the consumption of the higher positive valence of the nickel species i.e., Ni(III) by the EtOH. An evidence of this consumption may be developed if we consider the charge associated with the Ni(III) → Ni(II) transformation (i.e., under the cathodic peak) in the blank and in the presence of EtOH. The charge in both cases can be estimated from the area under the CV in the backward direction. It was found to be 2.60 and 0.71 mC in absence and presence of the EtOH, respectively. That is to say the consumed charge in the oxidation process decreases by about 72.7% in presence of EtOH. This may point to the electrocatalytic nature of EtOH oxidation on the Nano-CF/NiPh/GC [48]. Also, considerable anodic current is observed in the reverse sweep which can be assigned to further oxidation of EtOH. Since EtOH is oxidized concurrently with the Ni(II)/Ni(III) transformation and hence the oxidation products and intermediates block the active sites of the nickel species. After the higher anodic potential reached in the reverse sweep, these poisoning products may be removed and hence EtOH is reoxidized at the recovered surface in the reverse scan albeit with lower peak current. The latter is obtained since the recovery of the active sites may not be complete. For further explanation of the enhanced electrocatalytic behavior of Nano-CF/NiPh/GC over that of nano-NiPh, the electrochemically active surface area (ECSA) of the different electrodes was calculated from CVs of non-Faradic response (see the supplementary materials) and the consequent calculations of the electrochemical double-layer capacitance of the electrodes. The results in the Supplementary section show that ECSA of Nano-CF/NiPh/GC and nano-NiPh/GC was calculated to be 3.0 and 1.15 $cm^2$, respectively. The roughness factor (ECSA/$A_g$), where $A_g$ is the electrode geometrical area (0.07 $cm^2$) was calculated to be 42.3 and 16.4, respectively. Accordingly, the ECSA for Nano-CF/NiPh/GC is three-folds higher than that of the nano-NiPh/GC. This may help in explanation of the above enhancement of electrocatalytic properties of the Nano-CF/NiPh/GC towards ethanol oxidation.

Cyclic voltammetry responses of Nano-CF/NiPh/GC in 0.5 M NaOH containing 0.2 M EtOH at various potential sweep rates in the range of 5 to 1200 mV $s^{-1}$ are illustrated in Fig. 7A. The cathodic peak assigned for Ni(III) → Ni(II) transformation are not observed at low scan rates but it appears gradually and its value increases with the sweep rate. This observation may indicate that EtOH oxidation is considerably slower than the electrochemical oxidation of Ni(II) to higher valence Ni (III). Generally, the anodic peak current of EtOH oxidation increases with the potential sweep rate and the peak potential shifts to more positive potentials.

By the aid of the above CVs data in Fig. 7A, some kinetics and transport parameters can be determined. The value of $\alpha n_a$ can be calculated using the following equation [49];

$$E_p = K + \frac{RT}{2\alpha n_a F} \ln \nu \tag{6}$$

where $E_p$ is the peak potential, K is a constant and $F$ is the Faraday's constant, $R$ is the gas constant and $T$ is the absolute temperature. A plot of $E_p$ with ln $\nu$ gave a starlight line (plot is not shown). From the slope of such plot and using Eq. (6) the value of $\alpha n_a$ was calculated to be 0.24. The diffusion coefficient of EtOH can be determined from a plot of the peak current, $I_p$ with the square root of the scan rate, $\nu^{0.5}$ as depicted in Fig. 7B. A straight line is obtained ($R^2$ = 0.996) which is in accordance with the Randles-Sevcik equation for completely irreversible diffusion-controlled process [50]. The equation is given by;

$$I_p = 0.4961 \times nF\left(\frac{\alpha n_a F D_o}{RT}\right)^{0.5} ACv^{0.5} \tag{7}$$

The parameters appear in the above equation have the following

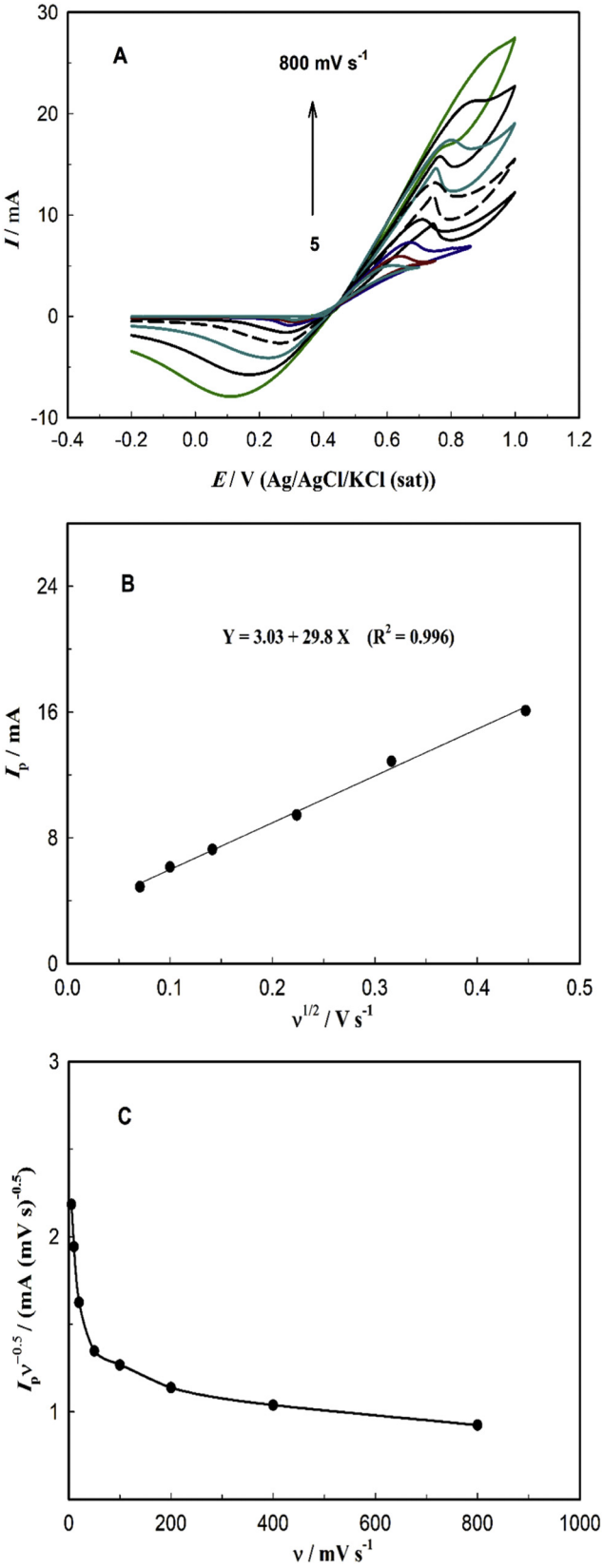


**Fig. 7.** (A) CV responses of Nano-CF/NiPh/GC in 0.5 M NaOH containing 0.2 M EtOH at different potential scan rates: From inner: 5, 10, 20, 50, 100, 200, 400, 800 mV $s^{-1}$. (B) Plot $I_p$ of EtOH electrochemical oxidation and the square of the scan rate, $\nu^{0.5}$. (C) Relation between $I_p$ $\nu^{-0.5}$ with the scan rate.

meaning. $A$ is the electrode surface area, $D_o$ is the diffusion coefficient of EtOH, $n$ is the total number of electrons ($n = 3$) [24], $C$ is the bulk concentration of EtOH and $\nu$ is the potential scan rate. Also, $\alpha$ is the charge transfer coefficient and $n_a$ is the number of electrons in the rate-determining step and the parameters $R$, $T$ and $F$ have their usual meanings. By using the slope of the straight line in Fig. 7B and the value of $\alpha n_a$ (calculated from Eq. (6)), the diffusion coefficient of EtOH, $D_o$ was determined from Eq. (7) to be $1.7 \times 10^{-5}\,cm^2\,s^{-1}$. This value is closer to those found in literatures [51, 52]. Fig. 7C shows a plot of $I_p.\nu^{-0.5}$ with the potential scan rate. It represents the characteristics features of typical catalyst regeneration mechanism in accordance with the results in Fig. 6. This can be suggested in the light of the catalyst regeneration mechanism during the electrocatalytic oxidation of ETOH on the Nano-CF/NiPh/GC [52]. In this context and considering the mechanism of ethanol oxidation in literatures [53, 54] and in the light of the present results, Ni(III) species act as electron transfer mediator for ethanol oxidation;

$$Ni(III) + EtOH \rightarrow Ni(II) + Products \quad (8)$$

where Ni(II) is oxidized again to Ni(III) at the prevailed anodic potential and hence it is regenerated.

### 3.3. Chronoamperometry study

Chronoamperometric measurements were also collected for further characterization of the Nano-CF/NiPh/GC for electrochemical oxidation of ethanol from alkaline solutions. The measurements can enable us to calculate the diffusion coefficient and the catalytic rate constant of EtOH. Fig. 8 shows chronoamperometric curves for Nano-CF/NiPh/GC in blank (0.5 M NaOH) (a) and 0.1 M EtOH (b) and 0.2 M EtOH (c) in 0.5 M NaOH. The current decreases rapidly at the start before it is stabilized at constant values. Also, the current increases with the increase in the [EtOH] which points to stable response to EtOH concentration. Cottrell equation is given by [55];

$$I = nF\,A\,D^{0.5}C\,\pi^{-0.5}t^{-0.5} \quad (9)$$

where $n$ is the number of electrons required for the conversion of one molecule of ETOH, $t$ is the time in seconds (s) and the remaining parameters have their usual meanings. The inset (I) of Fig. 8 depicts plots of the current, $I$ with $t^{-0.5}$ at two EtOH concentrations: 0.1 M (a) and 0.2 M (b) EtOH. The fitting equations of the straight lines are given on the figure. The slopes of the above lines were used to calculate the

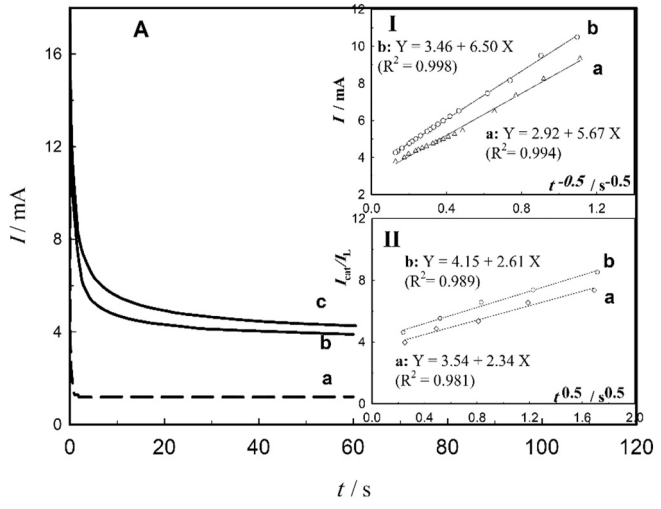


**Fig. 8.** (A) Chronoamperometric curves Nano-CF/NiPh/GC in blank (a), 0.1 M EtOH (b) and 0.2 M EtOH (c). The inset (I) shows the $I$-$t^{-0.5}$ plots for EtOH electrochemical oxidation in 0.5 M NaOH containing different EtOH concentrations: a) 0.1 and b) 0.2 M. The inset (II) shows the relation between $I_{cat}/I_L$ and $t^{0.5}$.

**Table 2**
Comparison of some parameters with literatures: catalytic rate constant, $k_{cat}$, peak potential, $E_{pa}$ and current density of the EtOH oxidation.

| Ref | Electrode | $E_p$/V (Ag/AgCl/KCl) | $I$/mA cm$^{-2}$ |
|---|---|---|---|
| (This work) | Nano-CF/NiPh/GC | 0.74 | 189 |
| [57] | Ni-carbon nanofibers | 0.75 | 60 |
| [58] | Activated carbon/nickel | 0.70 | 15 |
| [59] | Nickel/nitroaniline/MWCNT | 1.0 V | 32 |
| [60] | CNT–Ni | 0.70 | 0.5 |
| [61] | Poly-Ni | 0.61 | 16 |
| [62] | Ni-B nanotube | 0.65 | 19.5 |
| [32] | Nano-Ni/graphite | 1.0 | 162 |
| [63] | N-doped carbon/nickel | 0.70 | 210 |
| [64] | $Ni_xCo_{1-x}$/carbon nanofibers | 0.73 | 70 |
| [65] | MWCNT/$NiCo_2O_4$ | 0.75 | 26 |

ethanol diffusion coefficient. The latter was calculated to be $2.47 \times 10^{-5}$ and $8.1 \times 10^{-6}$ and for 0.1 M and 0.2 M EtOH, respectively. It may can be concluded that this value is comparable with that obtained from Eq. (7). On using the chronoamperogram curves shown in Fig. 8, the catalytic rate constant of EtOH oxidation can be calculated according to the following equation [56];

$$\frac{I_{cat}}{I_L} = \pi^{0.5}(k_{cat}C^o t)^{0.5} \quad (10)$$

where $I_{cat}$ and $I_L$ is the current in presence and absence of EtOH, respectively, and $C^o$ is the [EtOH] in mol cm$^{-3}$. Inset (II) depicts a plot of $I_{cat}/I_L$ with $t^{1/2}$ at two ethanol concentrations. Using the slopes of the straight lines in the figure, the average value of $k_{cat}$ was calculated to be $1.42 \times 10^4\,cm^3\,mol^{-1}\,s^{-1}$. This value is comparable with the literatures values [53].

In order to visualize the capability and advantages of the obtained results of the present electrode; Nano-CF/NiPh/GC for electrocatalytic oxidation of ethanol, the results here can be compared with literatures. The comparison is cited here in Table 2 for the current density, $I_p$, the peak potential, $E_p$ and the catalytic rate constant, $k_{cat}$. Inspection of the data in Table 2 lead to the fact the present electrode is better than some electrodes and comparable with others. The higher electrocatalytic properties of the; Nano-CF/NiPh/GC may stem from taking advantages of the stability of the Ni(II)/Ni(III) onto the phosphate structure. Meanwhile, compositing NiPh with the carbon nanofibers provide two distinctive characterizations; the higher adsorbability of the CF to ethanol and also to the great conductivity of the CF. These two important factors facilitates charge transfer as well as increasing the rate of electrochemical oxidation of ethanol on the Nano-CF/NiPh/GC electrode.

## 4. Conclusions

Carbon nanofibers/mesoporous NiPh (Nano-CF/NiPh) composite has been synthesized and applied for electrocatalytic of ethanol (EtOH) from alkaline 0.5 M NaOH solution at different experimental conditions. The material was characterized by different surface and electrochemical techniques. The diffusion coefficient of ethanol and catalytic rate constant were calculated to be $1.4 \times 10^{-5}\,cm^2\,s^{-1}$ and $4.5 \times 10^4\,cm^3\,mol^{-1}\,s^{-1}$, respectively. High performance of the fabricated modified electrode, Nano-CF/NiPh/GC was attributed to the increase in the material specific surface area, conductivity and an increase in the electrochemically active surface area due to presence of the carbon fibers and also due to higher adsorption extent of ethanol on the CF.

## Appendix A. Supplementary data

Supplementary data to this article can be found online at https://doi.org/10.1016/j.jelechem.2018.06.002.

## References


[1] D.R.M. Godoi, H.M. Villullas, F.-C. Zhu, Y.-X. Jiang, S.-G. Sun, J. Guo, L. Sun, R. Chen, A comparative investigation of metal-support interactions on the catalytic activity of Pt nanoparticles for ethanol oxidation in alkaline medium, J. Power Sources 311 (2016) 81–90.

[2] R. Varcoe, R.C.T. Slade, Prospects for alkaline anion-exchange membranes in low temperature fuel cells, J. Fuel Cells 5 (2005) 187–200.

[3] A.N. Geraldes, D.F. da Silva, E. Segura Pino, J.C. Martins Da Silva, R.F. Brambillade Souza, P. Hammer, E.V. Spinacé, A. Oliveira Neto, M. Linardi, M. Coelho dos Santos, Ethanol electro-oxidation in an alkaline medium using Pd/C, Au/C and PdAu/C electrocatalysts prepared by electron beam irradiation, Electrochim. Acta 111 (2013) 455–465.

[4] G.F. McLean, T. Niet, S. Prince-Richard, N. Djilali, An assessment of alkaline fuel cell technology, Int. J. Hydrog. Energy 27 (2002) 507–526.

[5] E. Antolini, Catalysts for direct ethanol fuel cells, J. Power Sources 170 (2007) 1–12.

[6] C. Xu, P. Kang Shen, Novel Pt/$CeO_2$/C catalysts for electrooxidation of alcohols in alkaline media, Chem. Commun. (19) (2004) 2238–2239.

[7] I. Mintsouli, J. Georgieva, S. Armyanov, E. Valova, G. Avdeev, A. Hubin, O. Steenhaut, J. Dille, D. Tsiplakides, S. Balomenou, S. Sotiropoulos, Pt-Cu electrocatalysts for methanol oxidation prepared by partial galvanic replacement of Cu/carbon powder precursors, Appl. Catal. B Environ. 136-137 (2013) 160–167.

[8] Y. Yu, Y. Hu, X. Liu, W. Deng, X. Wang, The study of Pt/Au electrocatalyst based on Cu under potential deposition and Pt redox replacement, Electrochim. Acta 54 (2009) 3092–3097.

[9] S.A. Grigoriev, E.K. Lyutikova, S. Martemianov, V.N. Fateev, On the possibility of replacement of Pt by Pd in a hydrogen electrode of PEM fuel cells, Int. J. Hydrog. Energy 32 (2007) 4438–4442.

[10] R. Bashyam, P. Zelenay, A class of non-precious metal composite catalysts for fuel cells, Nature 443 (2006) 63–66.

[11] P. Manivasakan, P. Ramasamy, J. Kim, Use of urchin-like $Ni_xCo_{3-x}O_4$ hierarchical nanostructures based on non-precious metals as bifunctional electrocatalysts for anion-exchange membrane alkaline alcohol fuel cells, Nano 6 (2014) 9665–9672.

[12] S.P.S. Badwal, S. Giddey, A. Kulkarni, J. Goel, S. Basu, Direct ethanol fuel cells for transport and stationary applications - a comprehensive review, Appl. Energy 145 (2015) 80–103.

[13] M.Z.F. Kamarudin, S.K. Kamarudin, M.S. Masdar, W.R.W. Daud, Review: direct ethanol fuel cells, Int. J. Hydrog. Energy 38 (2013) 9438–9453.

[14] K. Kakaei, Decoration of graphene oxide with Platinum Tin nanoparticles for ethanol oxidation, Electrochim. Acta 165 (2015) 330–337.

[15] N. Erini, R. Loukrakpam, V. Petkov, E.A. Baranova, R. Yang, D. Teschner, Y. Huang, S.R. Brankovic, P. Strasser, Ethanol electro-oxidation on ternary platinum–rhodium–tin nanocatalysts: insights in the atomic 3D structure of the active catalytic phase, ACS Catal. (6) (2014) 1859–1867.

[16] A.D. Modestov, M.R. Tarasevich, A.Yu. Leykin, V.Ya. Filimonov, MEA for alkaline direct ethanol fuel cell with alkali doped PBI membrane and non-platinum electrodes, J. Power Sources 188 (2009) 502–506.

[17] Y. Bai, Wu J, J. Xi, J. Wang, W. Zhu, L. Chen, X. Qiu, Electrochemical oxidation of ethanol on Pt–$ZrO_2$/C catalyst, Electrochem. Commun. 7 (2005) 1087–1090.

[18] Q. Yi, F. Niu, L. Sun, Fabrication of novel porous Pd particles and their electroactivity towards ethanol oxidation in alkaline media, Fuel 90 (2011) 2617–2623.

[19] R.H. Tammam, A.M. Fekry, M.M. Saleh, Electrocatalytic oxidation of methanol on ordered binary catalyst of manganese and nickel oxide nanoparticles, Int. J. Hydrog. Energy 40 (2015) 275–283.

[20] A.N. Golikand, S. Shahrokhian, M. Asgari, M.G. Maragheh, L. Irannejad, A. Khanchi, Electrocatalytic oxidation of methanol on a nickel electrode modified by nickel dimethylglyoxime complex in alkaline medium, J. Power Sources 144 (2005) 21–27.

[21] J. Wang, Q. Zhao, H. Hou, Y. Wu, W. Yu, X. Ji, L. Shao, Nickel nanoparticles supported on nitrogen-doped honeycomb-like carbon frameworks for effective methanol oxidation, RSC Adv. 7 (2017) 14152–14158.

[22] Y. Kang, W. Wang, Y. Pu, J. Li, D. Chai, Z. Lei, An effective Pd-NiOx-P composite catalyst for glycerol electrooxidation: co-existed phosphorus and nickel oxide to enhance performance of Pd, Chem. Eng. J. 308 (2017) 419–427.

[23] A. Kowal, S.N. Port, R.J. Nichols, Nickel hydroxide electrocatalysts for alcohol oxidation reactions: an evaluation by infrared spectroscopy and electrochemical methods, Catal. Today 38 (1997) 483–492.

[24] B. Ballarin, R. Seeber, D. Tonelli, A. Vaccari, Electrocatalytic properties of nickel(II) hydrotalcite-type anionic clay: application to methanol and ethanol oxidation, J. Electroanal. Chem. 463 (1999) 123–127.

[25] P.E. Sharel, L. Danqing, R.A. Lazenby, J. Sloan, M. Vidotti, P.R. Unwin, J.V. Macpherson, Electrodeposition of nickel hydroxide nanoparticles on carbon nanotube electrodes: correlation of particle crystallography with electrocatalytic properties, J. Phys. Chem. C 120 (29) (2016) 16059–16068.

[26] K. Raju, K.I. Ozoemena, Hierarchical one-dimensional ammonium nickel phosphate microrods for high-performance pseudocapacitors, Sci. Rep. 5 (2015) 1–13.

[27] Y. Li, C. Zhao, Iron-doped nickel phosphate as synergistic electrocatalyst for water oxidation, Chem. Mater. 28 (2016) 5659–5666.

[28] J. Yang, J. Tan, F. Yang, X. Li, X. Liu, D. Ma, Electro-oxidation of methanol on mesoporous nickel phosphate modified GCE, Electrochem. Commun. 23 (2012) 13–16.

[29] S.K. Hassaninejad-Darzi, M. Rahimnejad, M.G. Esfidvajani, Electrocatalytic oxidation of formaldehyde onto carbon paste electrode modified with nickel decorated nanoporous cobalt-nickel phosphate molecular sieve for fuel cell, Fuel Cells 16 (2016) 89–99.

[30] M.A. Al-Omair, A.H. Touny, F.A. Al-Odail, M.M. Saleh, Electrocatalytic oxidation of glucose at nickel phosphate nano/micro particles modified electrode, Electrocatalysis 8 (2017) 340–350.

[31] M.A. Al-Omair, A.H. Touny, M.M. Saleh, Reflux-based synthesis and electrocatalytic characteristics of nickel phosphate nanoparticles, J. Power Sources 342 (2017) 1032–1039.

[32] A.B. Soliman, H.S. Abdel-Samad, S.S. Abdel Rehim, M.A. Ahmed, H.H. Hassan, High performance nano-Ni/graphite electrode for electro-oxidation in direct alkaline ethanol fuel cells, J. Power Sources 325 (2016) 653–663.

[33] K. Kakaei, K. Marzang, One – step synthesis of nitrogen doped reduced graphene oxidewith NiCo nanoparticles for ethanol oxidation in alkaline media, J. Colloid Interface Sci. 462 (2016) 148–153.

[34] Z. Liu, Z. Li, F. Wang, J. Liu, J. Ji, J. Wang, W. Wang, S. Qin, L. Zhang, Synthesis of multi-walled carbon nanotube supported nickel catalysts by hydrazine reduction and their electrocatalytic activity on ethanol electro-oxidation, Mater. Lett. 65 (2011) 3396–3398.

[35] M. Shamsipur, M. Najafi, M. Reza, M. Hosseini, Highly improved electrooxidation of glucose at a nickel(II) oxide/multi-walled carbon nanotube modified glassy carbon electrode, Bioelectrochemistry 77 (2010) 120–124.

[36] X. Tong, Y. Qin, X. Guo, O. Moutanabbir, X. Ao, E. Pippel, L. Zhang, M. Knez, Enhanced catalytic activity for methanol electrooxidation of uniformly dispersed nickel oxide nanoparticles-carbon nanotube hybrid materials, Small 8 (22) (2012) 3390–3395.

[37] A.H. Touny, Reham H. Tammam, M.M. Saleh, Electrocatalytic oxidation of formaldehyde on nanoporous nickel phosphate modified electrode, Appl. Catal. B Environ. 224 (2018) 1017–1026.

[38] National Bureau of Standards Monograph 25, Section 19-Data for 51 Substances Natl. Bur. Stand. (U.S.), Monograph. 25-Sec. 19, 118 pages, (Dec. 1982) (CODEN: NBSMA6).

[39] K.A. Cychosz, R. Guillet-Nicolas, J. Garcıa-Martınez, M. Thommes, Recent advances in the textural characterization of hierarchically structured nanoporous materials, Chem. Soc. Rev. 46 (2017) 389–414.

[40] K.S.W. Sing, D.H. Evertt, R.A.W. Haul, L. Moscou, R.A. Pierotti, J. Rouquerol, T. Siemieniewska, Reporting physisorption data for gas/solid systems with special references to the determination of surface area and porosity, Pure Appl. Chem. 57 (1985) 603–619.

[41] L. Kong, W. Chen, Ionic liquid directed mesoporous carbon nanoflakes as an efficient electrode material, Sci. Rep. 5 (2015) 18236–18245.

[42] Y. Zhan, M. Lu, S. Yang, Z. Liu, J. Yang Lee, The origin of catalytic activity of nickel phosphate for oxygen evolution in alkaline solution and its further enhancement by iron substitution, ChemElectroChem 3 (2016) 615–621.

[43] Y. Zhao, Z. Chen, D. Bang Xiong, Y. Qiao, Y. Tang, F. Gao, Hybridized phosphate with ultrathin nanoslices and single crystal microplatelets for high performance supercapacitors, Sci. Rep. 6 (2016) 1–10.

[44] R.H. Tammam, M.M. Saleh, On the electrocatalytic urea oxidation on nickel oxide nanoparticles modified glassy carbon electrode, J. Electroanal. Chem. 794 (2017) 189–196.

[45] S.N. Azizi, S. Ghasemi, H. Yazdani-Sheldarrei, Synthesis of mesoporous silica (SBA-16) nanoparticles using silica extracted from stem cane ash and its application in electrocatalytic oxidation of methanol, Electrochim. Acta 190 (2016) 118–125.

[46] J. Taraszewska, G. Roslonek, Electrocatalytic oxidation of methanol on a glassy carbon electrode modified by nickel hydroxide formed by ex-situ chemical precipitation, J. Electroanal. Chem. 364 (1994) 209–213.

[47] L. Zheng, J.F. Song, Electrocatalytic oxidation of methanol and other short chain aliphatic alcohols at Ni(II)-quercetin complex modified multi-wall carbon nano tube paste electrode, J. Solid State Electrochem. 14 (2010) 43–50.

[48] S.K.H. Darzi, M.G. Esfidvajani, Electrocatalytic oxidation of ethanol using modified nickel phosphate nanoparticles and multi-walled carbon nanotubes paste electrode in alkaline media for fuel cell, Int. J. Hydrog. Energy 41 (2016) 20085–20099.

[49] L. Jiang, R. Wang, X. Li, L. Jiang, G. Lu, Electrochemical oxidation behavior of nitrite on a chitosan-carboxylated multiwall carbon nanotube modified electrode, Electrochem. Commun. 7 (2005) 597–601.

[50] F. Xiao, F. Zhao, J. Li, R. Yan, J. Yu, B. Zeng, Sensitive voltammetric determination of chloramphenicol by using single-wall carbon nanotube–gold nanoparticle–ionic liquid composite film modified glassy carbon electrodes, Anal. Chim. Acta 596 (2007) 79–85.

[51] CRC Handbook of Chemistry and Physics, 84th ed., (2003–2004) (Table 6–181).

[52] A. Ehsani, M.G. Mahjani, M. Jafarian, A. Naeemy, Electrosynthesis of polypyrrole composite film and electrocatalytic oxidation of ethanol, Electrochim. Acta 71 (2012) 128–133.

[53] J. Zhan, M. Cai, C. Zhang, C. Wang, Synthesis of mesoporous $NiCo_2O_4$ fibers and their electrocatalytic activity on direct oxidation of ethanol in alkaline media, Electrochim. Acta 154 (2015) 70–76.

[54] J.-W. Kim, Park, Electrochemical oxidation of ethanol at nickel hydroxide electrodes in alkaline media studied by electrochemical impedance spectroscopy, J. Korean Electrochem. Soc. 8 (2005) 117–124.

[55] F.T. Javazmi, M.S. Nooshabadi, H.K. Maleh, Analysis of glutathione in the presence of acetaminophen and tyrosine via an amplified electrode with MgO/SWCNTs as a sensor in the hemolyzed erythrocyte, Talanta 176 (2018) 208–213.

[56] M. Doulache, A. Benchettara, M. Trari, Detection of salicylic acid by electrocatalytic oxidation at a nickel-modified glassy carbon electrode, J. Anal. Chem. 69 (2014) 51–56.

[57] N.A.M. Barakat, H.M. Moustafa, M.M. Nassar, M.A. Abdelkareem, M.S. Mahmoud, A.A. Almajid, K.A. Khalil, Distinct influence for carbon nano-morphology on the activity and optimum metal loading of Ni/C composite used for ethanol oxidation,

Electrochim. Acta 182 (2015) 143–155.
[58] A. Cuna, C.R. Plascencia, E.L. da Silva, J. Marcuzzo, S. Khan, N. Tancredi, M.R. Baldan, C. de Fraga Malfatti, Electrochemical and spectroelectrochemical analyses of hydrothermal carbon supported nickel electrocatalyst for ethanol electrooxidation in alkaline medium, Appl. Catal. B Environ. 202 (2017) 95–103.
[59] G. Ping Jin, Y.-F. Ding, P. Pei Zheng, Electrodeposition of nickel nanoparticles on functional MWCNT surfaces for ethanol oxidation, J. Power Sources 166 (2007) 80–86.
[60] N.M. Suleimanov, S.M. Khantimerov, E.F. Kukovitsky, V.L. Matukhin, Electrooxidation of ethanol on carbon nanotubes-nickel nanoparticles composites in alkaline media, J. Solid State Electrochem. 12 (2008) 1021–1023.
[61] A.F.B. Barbosa, V.L. Oliveira, J. van Drunen, G. Tremiliosi-Filho, Ethanol electrooxidation reaction using a polycrystalline nickel electrode in alkaline media: temperature influence and reaction mechanism, J. Electroanal. Chem. 746 (2015) 31–38.
[62] F. Muench, M. Oezaslan, M. Rauber, S. Kaserer, A. Fuchs, E. Mankel, J. Brötz, P. Strasser, C. Roth, W. Ensinger, Electroless synthesis of nanostructured nickel and nickel-boron tubes and their performance as unsupported ethanol electrooxidation catalysts, J. Power Sources 222 (2013) 243–252.
[63] W. Shi, Q. Wang, F. Qin, J. Yu, M. Jia, H. Gao, Y. Zhang, Y. Zhao, G. Li, N-doped carbon encapsulated nickel nanoparticles: rational fabrication and ultra-high performance for ethanol oxidation, Electrochim. Acta 232 (2017) 332–338.
[64] N.A.M. Barakat, M. Motlak, A.A. Elzatahry, K.A. Khalil, E.A.M. Abdelghani, $Ni_xCo_{1-x}$ alloy nanoparticle-doped carbon nanofibers as effective non-precious catalyst for ethanol oxidation, Int. J. Hydrog. Energy 39 (2014) 305–316.
[65] S.S. Jayaseelan, T. Hoon Ko, S. Radhakrishnan, C. Min Yang, H. Yong Kim, B. Suhk Kim, Novel MWCNT interconnected $NiCo_2O_4$ aerogel prepared by a supercritical $CO_2$ drying method for ethanol electrooxidation in alkaline medium, Int. J. Hydrog. Energy 41 (2016) 13504–13512.